

# Kinetic modeling of pure hydrogen production from decalin

Bo Wang<sup>a</sup>, D. Wayne Goodman<sup>a</sup>, Gilbert F. Froment<sup>b,\*</sup>

<sup>a</sup> Department of Chemical Engineering, Texas A&M University, College Station, TX 77843-3122, USA

<sup>b</sup> Department of Chemistry, Texas A&M University, College Station, TX 77842, USA

Received 10 August 2007; revised 12 November 2007; accepted 13 November 2007

## Abstract

We investigate the dehydrogenation of decalin for the production of pure hydrogen for fuel cell applications. Supported Pt catalysts can achieve about 98% conversion with >99.9% selectivity for the dehydrogenation reaction. Cracking reactions occur only at high temperature. The partially dehydrogenated product, tetralin, was formed with a molar selectivity <6%, depending on the operating conditions. We investigated the kinetics of the dehydrogenation of decalin in a fixed-bed tubular reactor at 275–345 °C and atmospheric pressure. A Hougen–Watson-type kinetic model accounted for the dehydrogenation of *cis*- and *trans*-decalin as well as the isomerization between the two isomers, the formation of the intermediate tetralin and the final product, naphthalene. The rigorous discrimination between rival models led to parameter values that are statistically significant and satisfied the physicochemical criteria.

© 2007 Elsevier Inc. All rights reserved.

**Keywords:** Hydrogen; Fuel cell; Dehydrogenation; Decalin; Kinetics

## 1. Introduction

Fuel cells have the potential to replace the internal combustion engine in vehicles, offering cleaner, more efficient alternatives to the combustion of gasoline and other fossil fuels [1–5]. The distribution and onboard storage of hydrogen are serious disadvantages for the application of fuel cells. Today, hydrogen is produced primarily by catalytic steam reforming of natural gas and other hydrocarbons [6,7]. The reforming of hydrocarbons produces CO as a byproduct, and its presence poisons the Pt-based electrocatalysts used in PEM fuel cells, so that the hydrogen must be purified. Another promising technology for storing and transporting hydrogen is the dehydrogenation of organic hydrocarbons with high hydrogen content. Hydrocarbons such as cyclohexane, methylcyclohexane, and decalin have been considered for this purpose [8–12]. Only hydrogen and dehydrogenated hydrocarbons are formed as the main products in this reaction. The absence of any substantial amount of carbon oxides eliminates the need for further purification of the

hydrogen. Another advantage of using these liquid hydrocarbons as hydrogen storage media is that the present infrastructures, such as gas stations and oil tankers, can be used for their storage and transportation. The dehydrogenation of cycloalkanes is a reversible process. The products (e.g., benzene, toluene, naphthalene) can be hydrogenated back to cycloalkanes in specialized gas stations.

A number of supported metal catalysts have been reported in the literature for the dehydrogenation of cycloalkane. Somorjai and co-workers studied the dehydrogenation of cyclohexane over single-crystal Sn/Pt(111) and Pt(111)/Sn/K in a vacuum chamber at 573 K [14]. It was found that the adsorption of tin and potassium on Pt(111) decreased deactivation of the surface by coke deposition, as well as the turnover rate of cyclohexane dehydrogenation, due to site coverage. Ichikawa and co-workers investigated the dehydrogenation of cyclohexane, methylcyclohexane, and decalin over activated carbon-supported Ni, Pt and Ni–Pt catalysts using a spray pulse mode reactor operating at 287–375 °C [8,9]. It was assumed that pulse spray operation could increase the reaction rate by suppressing the reverse reaction. The conversions amounted to 25–35%, with a >98.8% selectivity for dehydrogenation re-

\* Corresponding author.

E-mail address: [g.froment@che.tamu.edu](mailto:g.froment@che.tamu.edu) (G.F. Froment).

actions. Saito and co-workers performed dehydrogenation of decalin at 210 °C with carbon-supported Pt based catalysts in a batch-type reactor with continuous removal of the produced hydrogen through the condenser [10]. After 2.5 h of operation, the conversions were in the range of 25.4–35.8%. Okada et al. also reported their results for alumina-supported Pt catalysts in methylcyclohexane dehydrogenation in a fixed-bed reactor [11]. This catalyst could generate hydrogen from methylcyclohexane with a conversion of 95% and toluene selectivity >99.9% at 320 °C. Recently, Huffman and co-workers used stacked-cone carbon nanotubes (SC-CNTs) as a support to prepare Pt catalysts for the dehydrogenation of cycloalkanes [12,13]. The catalysts exhibited 100% selectivity for the dehydrogenation reactions at 240 °C. It was reported that Pt and Pd were more highly dispersed on SC-CNT than on the other supports, such as granular carbon and  $\gamma$ -Al<sub>2</sub>O<sub>3</sub>, thus resulting in higher catalytic activity. The dehydrogenation rate of decalin into tetralin was slower than the dehydrogenation of tetralin. In addition, *cis*-decalin exhibited a higher conversion rate than *trans*-decalin because of its flexible geometric structure. The regeneration of the deactivated carbon supported catalyst is a problem and limits its application.

The gravimetric hydrogen content is higher in decalin than in cyclohexane, and the dehydrogenated product, naphthalene, is environmentally favorable. These advantages make decalin a good candidate for a hydrogen carrier. The present study investigated the dehydrogenation of decalin. Catalysts and operating conditions were optimized, and a rigorous kinetic model was derived. This is a valuable tool for scaling-up the process and guiding its operation.

## 2. Experimental

### 2.1. Feed mixtures

Decalin, purchased from Aldrich, consisted of 24% *cis*-isomers and 76% *trans*-isomers. The purity of the H<sub>2</sub>, Ar, and N<sub>2</sub> amounted to 99.99%.

### 2.2. Catalyst preparation

Supported Pt catalysts were used in the dehydrogenation of cycloalkanes. Three different kinds of high-surface area supports were used:  $\gamma$ -alumina, silica, and activated carbon. The catalyst was prepared by adding a certain amount of aqueous H<sub>2</sub>PtCl<sub>6</sub> solution to the support and impregnating it at 80 °C for 2 h. The resulting Pt/support catalyst was dried in air at 130 °C, then calcined at 500 °C for 3 h. Sn was added to the supported Pt catalyst through evaporative impregnation of a certain amount of nitric solution of tin chloride at 80 °C for 2 h, dried at 130 °C, and then calcined at 500 °C for 3 h. Before the reaction, the catalyst was activated first by removing water at 500 °C for 2 h, followed by reduction at 500 °C with hydrogen. The catalysts were tested for a particle size <0.1 mm. According to the extension of the Weisz and Prater criterion, based on the generalized modulus [15], diffusional limitations can be ne-

glected when

$$\Phi = \frac{(r_i \rho_s)_{\text{obs}} L^2 g(C_s^s)}{2 \int_{C_{s,\text{eq}}}^{C_s^s} D_e(C) g(C) dC} \ll 1,$$

in which  $g(C)$  represents the concentration-dependent part of the rate equation. The diffusivity of decalin in the reaction mixtures,  $D_e$ , is calculated to be 0.27 cm<sup>2</sup>/s. The calculated values of  $\Phi$  for the dehydrogenation of TDC and CDC on 0.1-mm catalyst pellets are 0.01 and 0.04, indicating negligible intraparticle diffusional limitation. The operating conditions were also chosen to avoid external mass and heat transfer limitations. Thus, intrinsic kinetics were derived.

### 2.3. Fixed-bed reactor setup

The dehydrogenation of decalin was carried out on supported Pt catalyst in a fixed-bed reactor operating at atmospheric pressure (Fig. 1). The gas feeds (H<sub>2</sub>, N<sub>2</sub>, and air for regeneration of the deactivated catalyst) were controlled by mass flow controllers. The liquid was fed by a reciprocating pump. The liquid feed was vaporized in the packed mixing chamber and mixed with other gas streams before flowing to the reactor. The reactor was a 1.2-cm-i.d. stainless steel tube heated by a tubular furnace. The reactor axial temperature profile was monitored by a sliding thermocouple. The reaction products were analyzed by a HP 5890 online gas chromatograph equipped with a thermal conductivity detector (TCD) and a flame ionization detector (FID). HP-5 capillary columns with an FID were used to analyze the hydrocarbon components. The 13X packed column connected to a TCD was used to detect H<sub>2</sub>. Argon was used as the carrier gas, and the flow rate was maintained at 30 mL/min. N<sub>2</sub> was fed into the feed stream as an internal standard to calibrate the hydrogen flow. The exit flow rate of hydrogen was measured by a bubble meter. For accurate gas chromatography (GC) analysis, the transfer line from the reactor exit to the gas chromatograph and the sampling valve were insulated to keep the reactor effluent in the gas state.

## 3. Results

### 3.1. Definition of conversions and selectivities

Conversion of *trans*-decalin (TDC),

$$X_{\text{TDC}} = \frac{(\text{moles of TDC in}) - (\text{moles of TDC out})}{\text{moles of TDC in}} \times 100.$$

Conversion of *cis*-decalin (CDC),

$$X_{\text{CDC}} = \frac{(\text{moles of CDC in}) - (\text{moles of CDC out})}{\text{moles of CDC in}} \times 100.$$

Conversion of decalin into tetralin (TT),

$$X_{\text{TT}} = \frac{\text{moles of TT out}}{\text{moles of DC in}} \times 100.$$

Conversion of TDC and CDC into naphthalene (NP),

$$X_{\text{NP}} = \frac{\text{moles of NP out}}{\text{moles of DC in}} \times 100.$$

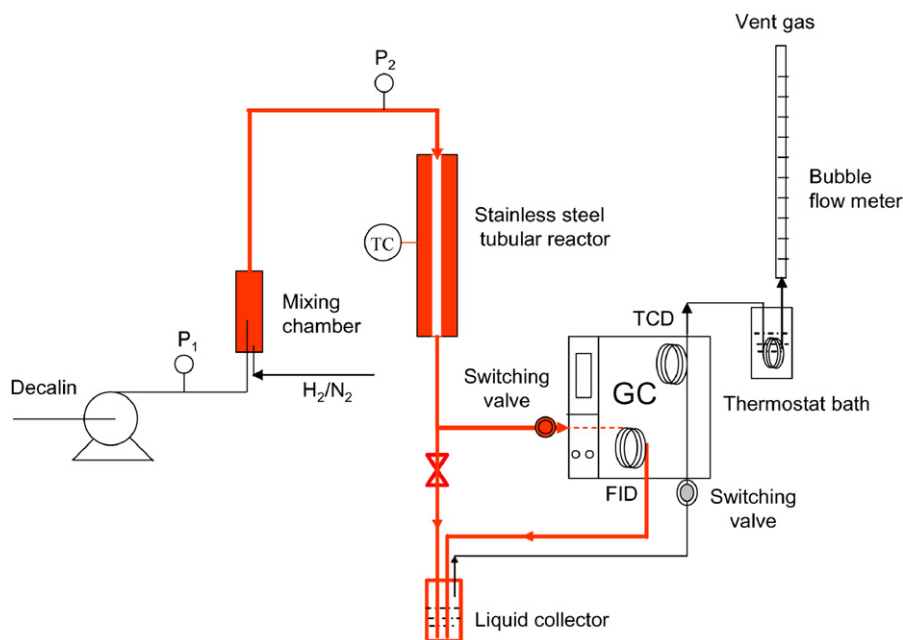


Fig. 1. Fixed-bed experimental setup for the production of H<sub>2</sub> from decalin.

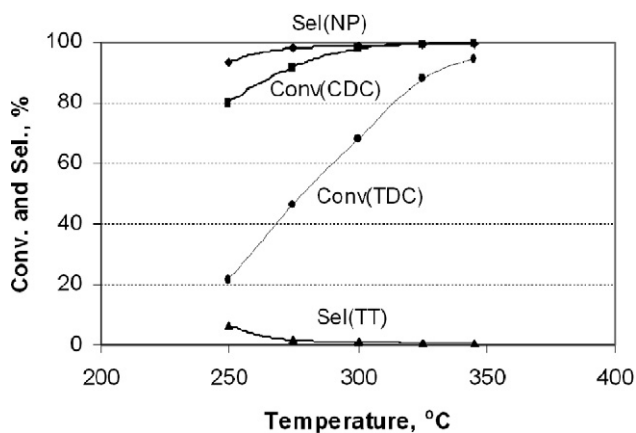


Fig. 2. Effect of temperature on decalin dehydrogenation (the lines correspond to a visual fit of the experimental data). Operating conditions: 0.8 wt% Pt/ $\gamma$ -alumina, space time = 60 kg<sub>cat</sub> h/kmol, H<sub>2</sub>/cyclohexane = 1.

$$\text{Selectivity} = \frac{\text{moles of product } i \text{ formed}}{\text{moles of DC converted}} \times 100,$$

where *i* refers to TT or NP selectivity for products.

### 3.2. Effect of temperature

The decalin feed consisted of 24% *cis*-isomers and 76% *trans*-isomers. The dehydrogenation was performed at atmospheric pressure, 250–350 °C, a space-time of 60 g<sub>cat</sub> h/mol, and a hydrogen-to-decalin molar ratio of 1. Fig. 2 shows that the conversion of *cis*-decalin was much higher than that of the *trans*-isomer; for example, the conversions of *cis*-decalin and *trans*-decalin at 300 °C were 98.0 and 66.8%, respectively. Two factors may contribute to this: (1) the *cis*-isomer was more active in the dehydrogenation reaction, and (2) isomerization occurred on the acid sites of the  $\gamma$ -alumina, and the rate of isomerization of *cis*-isomer into *trans*-isomer was much higher

than the reverse reaction. The conversions of both decalin isomers increased with temperature. The selectivity for naphthalene was much higher than that of tetralin. With a temperature increase from 250 to 350 °C, the selectivity for naphthalene increased from 93.6 to 99.7%, whereas, the selectivity for tetralin decreased from 6.4 to 0.3%. Tetralin is the intermediate product in decalin dehydrogenation. It can be further dehydrogenated at higher temperature to additional hydrogen.

### 3.3. Catalyst stability

The stability of 0.8 wt% Pt–0.3 wt% Sn/ $\gamma$ -alumina catalyst in decalin dehydrogenation was tested in both the absence and the presence of hydrogen at 340 °C and a space-time of 80 kg<sub>cat</sub> h/kmol. As shown in Fig. 3, the conversion decrease from the original 98.8 to 95.4% after 40 h, but showed no apparent decrease after 30 h when hydrogen was co-fed.

### 3.4. Effect of space-time

For a fixed temperature and a H<sub>2</sub>/decalin molar ratio of 1, the feed rate of decalin was varied to investigate the effect of the space-time on the conversion. Fig. 4 shows an example of the conversions of *cis*- and *trans*-decalin and the conversions into tetralin and naphthalene as a function of space-time at 325 °C. (The points represent the experimental data. The curve is discussed later.) It can be seen that the conversions of *cis*- and *trans*-decalin, and the conversion into naphthalene, increased with space-time. The conversion into tetralin was <2.0%. Similar experiments were carried out at 345, 300, and 275 °C.

### 3.5. Effect of the H<sub>2</sub>/decalin molar ratio

Whereas the co-feed of hydrogen inhibits catalyst deactivation, it also may decrease the conversion of the dehydrogenation

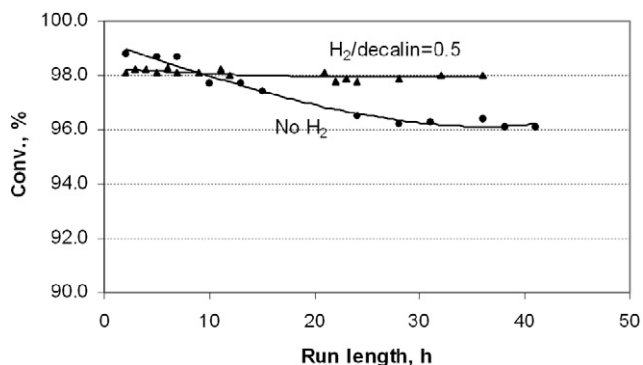


Fig. 3. Stability of the catalyst in decalin dehydrogenation at 340 °C and space time = 80 kg<sub>cat</sub> h/kmol (the lines correspond to a visual fit of the experimental data).

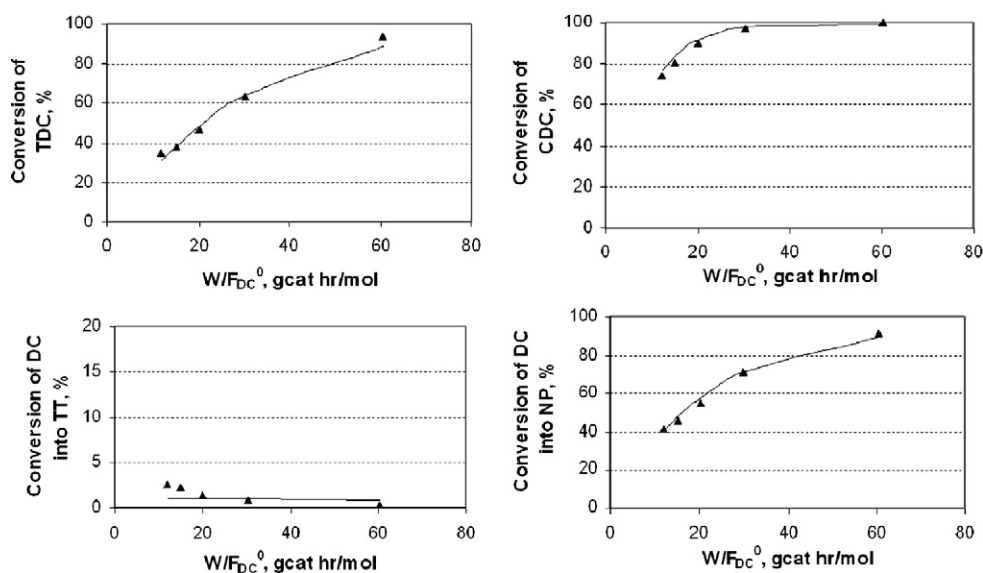


Fig. 4. Comparison of experimental (▲) and calculated (—) conversions as a function of space time at 325 °C for retained model, case I-2).

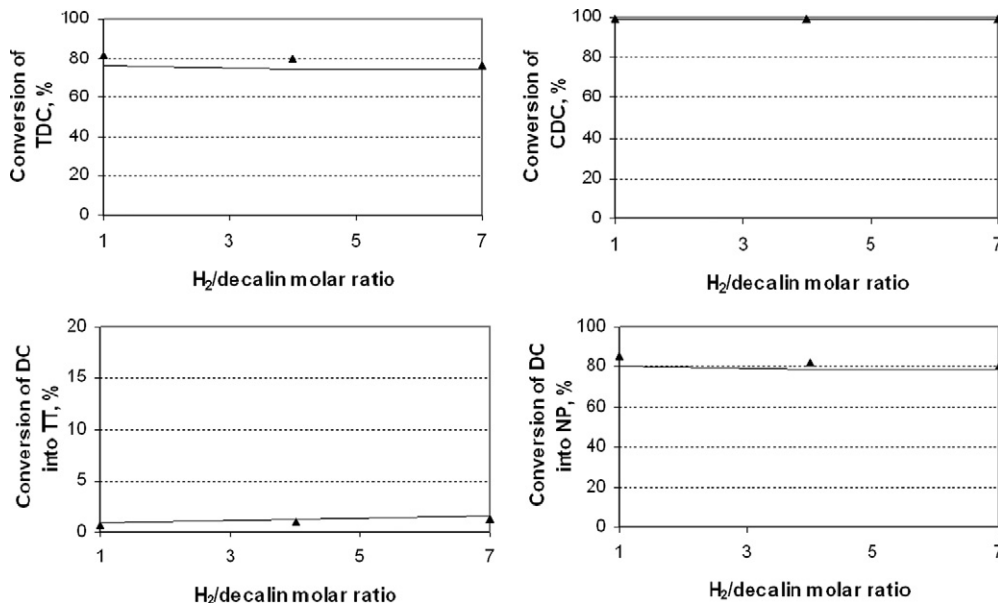


Fig. 5. Comparison of experimental (▲) and calculated (—) conversions as a function of H<sub>2</sub>/decalin molar ratio at 325 °C and space time of 40 kg<sub>cat</sub> h/kmol for case I-2).

reaction. Holding the space-time and temperature constant, the H<sub>2</sub>/decalin molar ratio was varied from 1 to 7 to check the effect of H<sub>2</sub> on the conversion. Fig. 5 shows the conversions as a function of ratio at 325 °C and space-time of 60 g<sub>cat</sub> h/mol. (Points represent the experimental data. The curve is discussed later.) The conversions of *cis*- and *trans*-decalin and naphthalene decreased with an increasing H<sub>2</sub>/decalin molar ratio, whereas the conversion to tetralin increased with an increasing H<sub>2</sub>/decalin molar ratio. Tetralin is the intermediate product in decalin dehydrogenation. The co-feed of H<sub>2</sub> may inhibit the further dehydrogenation of tetralin more than its conversion from decalin, and thus increase the conversion into the intermediate product, tetralin.

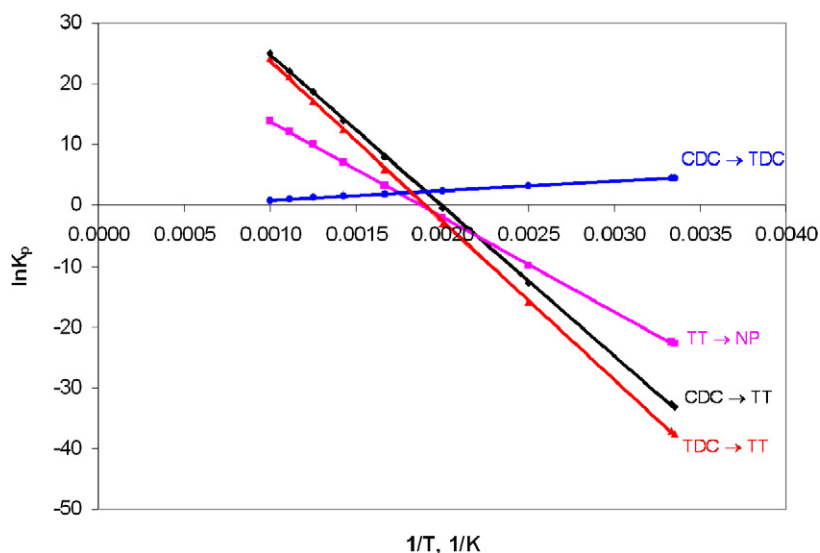


Fig. 6. Values of the equilibrium constants of the reactions involved in the dehydrogenation of decalin.

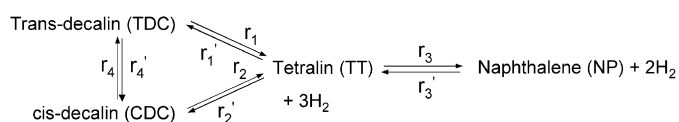
## 4. Kinetic modeling

### 4.1. Thermodynamic aspects

The equilibrium constant of each possible reaction in the dehydrogenation of decalin is shown in Fig. 6. Four possible reactions are involved in the dehydrogenation of decalin. Both *cis*- and *trans*-decalin can be dehydrogenated to form the intermediate product tetralin that can be further dehydrogenated to form the final product, naphthalene. The equilibrium constants at 325 °C for the isomerization of *cis*-decalin to *trans*-decalin and the reverse reaction were 7.40 and 0.135, respectively, meaning that the isomerization of *cis*- into *trans*- will be favored over the reverse reaction. The equilibrium constants at 275 °C for the dehydrogenation reactions of *cis*-decalin into tetralin, *trans*-decalin into tetralin, and tetralin into naphthalene were 77.08, 8.23, and 2.66, respectively. This means that the reverse reaction could not be neglected. Furthermore, the equilibrium constants of all of the dehydrogenation reactions increased with temperature, whereas the equilibrium constant of *cis*- into *trans*-isomerization decreased with temperature. Consequently, high temperatures will favor dehydrogenation, and low temperature will favor the isomerization of *cis*-decalin to *trans*-decalin.

### 4.2. Reaction scheme

Two kinds of active sites—metal sites and acid sites—are involved in the dehydrogenation of decalin over Pt–Sn/ $\gamma$ -Al<sub>2</sub>O<sub>3</sub>. A possible reaction scheme for the dehydrogenation of decalin based on the foregoing thermodynamic calculations is shown in Scheme 1. Both *cis*-decalin and *trans*-decalin can be dehydrogenated to form tetralin and H<sub>2</sub>. Tetralin can be further dehydrogenated to form the final product, naphthalene, thus generating more H<sub>2</sub>. At the same time, the isomerization be-



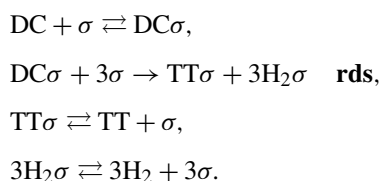
Scheme 1. Reaction scheme for the dehydrogenation of decalin.

tween the two decalin isomers occurs over the acid active site. All of these reactions are reversible.

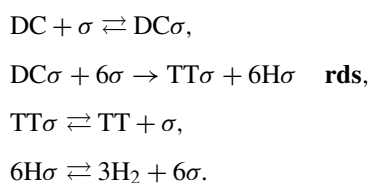
### 4.3. Rate equations

When the surface reactions of the adsorbed decalins, tetralin, and naphthalene are the rate-determining steps (RDSs), the dehydrogenation rates on the Pt sites can be formulated for case I, in which three hydrogen molecules are removed simultaneously in the RDS. Rate equations can be further discriminated between molecular (case I-1) and dissociative desorption of hydrogen in the RDS (case I-2).

Case I-1 (Molecular desorption of hydrogen in the RDS):



Case I-2 (Dissociative desorption of hydrogen in the RDS):



For molecular desorption of hydrogen, the dehydrogenation rates on the Pt active sites can be written as

$$\begin{aligned} r_1 &= k_{sr1} K_{TDC} P_{TDC} / \Delta^4, \\ r_2 &= k_{sr2} K_{CDC} P_{CDC} / \Delta^4, \\ r_3 &= k_{sr3} K_{TT} P_{TT} / \Delta^3. \end{aligned} \quad (1)$$

The reverse (hydrogenation) rates on the Pt sites can be written as

$$\begin{aligned} r'_1 &= k'_{sr1} K_{TT} K_{H_2} P_{TT} P_{H_2}^3 / \Delta^4, \\ r'_2 &= k'_{sr2} K_{TT} K_{H_2} P_{TT} P_{H_2}^3 / \Delta^4, \\ r'_3 &= k'_{sr3} K_{NP} K_{H_2} P_{NP} P_{H_2}^2 / \Delta^3. \end{aligned} \quad (2)$$

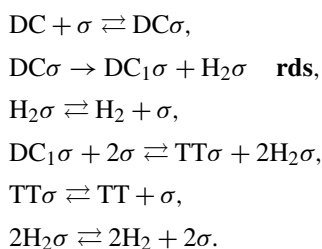
The  $\Delta$  appearing in the denominator of the above reaction rates is

$$1 + K_{CDC} P_{CDC} + K_{TDC} P_{TDC} + K_{TT} P_{TT} + K_{H_2} P_{H_2} + K_{NP} P_{NP}. \quad (3)$$

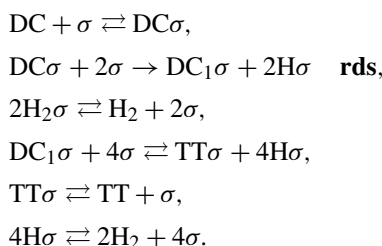
As the numbers of active sites involved in the RDSs of the dehydrogenations of TDC, CDC, and TT in the case of molecular desorption of hydrogen are 4, 4, and 3, the exponents appearing in the denominator of rate equations  $r_1$ ,  $r_2$ , and  $r_3$  are 4, 4, and 3, respectively. The same holds true for the reverse reactions with rates  $r'_1$ ,  $r'_2$ , and  $r'_3$ .

When hydrogen is dissociatively desorbed in the RDS on Pt active sites, the dehydrogenation and reverse hydrogenation rate equations are similar. But the hydrogen term in the denominator becomes  $(K_{H_2} P_{H_2})^{1/2}$ . In addition, because the numbers of active sites involved in the RDSs of the dehydrogenation of TDC, CDC, and TT in the dissociative desorption of hydrogen are 7, 7, and 5, respectively, the exponents appearing in the denominator of rate equations  $r_1$ ,  $r_2$ , and  $r_3$  are 7, 7, and 5, respectively. The same holds for the reverse reactions with rates  $r'_1$ ,  $r'_2$ , and  $r'_4$ .

Case II-1 (Molecular desorption of hydrogen in the RDS):



Case I-2 (Dissociative desorption of hydrogen in the RDS):



In case II, the removal of the first hydrogen is assumed to be the RDS. The partially dehydrogenated species are then sub-

jected to further dehydrogenation to remove the remaining hydrogen. As in case I, the dehydrogenation rate on Pt sites can be considered to occur with molecular or dissociative desorption of hydrogen in the RDS. For molecular desorption of hydrogen (case II-1), the dehydrogenation rate on Pt active sites can be written as

$$\begin{aligned} r_1 &= k_{sr1} K_{TDC} P_{TDC} / \Delta^2, \\ r_2 &= k_{sr2} K_{CDC} P_{CDC} / \Delta^2, \\ r_3 &= k_{sr3} K_{TT} P_{TT} / \Delta^2, \end{aligned} \quad (4)$$

and the reverse (hydrogenation) rates on Pt sites can be written as

$$\begin{aligned} r'_1 &= k'_{sr1} K_{TT} K_{H_2} P_{TT} P_{H_2}^3 / \Delta^2, \\ r'_2 &= k'_{sr2} K_{TT} K_{H_2} P_{TT} P_{H_2}^3 / \Delta^2, \\ r'_3 &= k'_{sr3} K_{NP} K_{H_2} P_{NP} P_{H_2}^2 / \Delta^2. \end{aligned} \quad (5)$$

The  $\Delta$ 's appearing in the denominator in the foregoing reaction rates are

$$\begin{aligned} \Delta &= 1 + K_{CDC} P_{CDC} + K_{TDC} P_{TDC} + K_{TT} P_{TT} + K_{H_2} P_{H_2} \\ &\quad + K_{NP} P_{NP} + K_{TT} P_{TT} K_{H_2}^2 P_{H_2}^2 / K_{DC1} \\ &\quad + K_{NP} P_{NP} K_{H_2} P_{H_2} / K_{TT1} \end{aligned} \quad (6)$$

for removal of the remaining two hydrogens simultaneously, and

$$\begin{aligned} \Delta &= 1 + K_{CDC} P_{CDC} + K_{TDC} P_{TDC} + K_{TT} P_{TT} + K_{H_2} P_{H_2} \\ &\quad + K_{NP} P_{NP} + K_{TT} P_{TT} K_{H_2}^2 P_{H_2}^2 / (K_{DC1} K_{DC2}) \\ &\quad + K_{TT} P_{TT} K_{H_2} P_{H_2} / K_{DC2} + K_{NP} P_{NP} K_{H_2} P_{H_2} / K_{TT1} \end{aligned} \quad (7)$$

for removal of the remaining two hydrogens in two steps. But, given the selection of the RDSs, the partially dehydrogenated species are present in very low concentrations, so that they can be neglected in the denominator. The denominator then can be written as

$$1 + K_{CDC} P_{CDC} + K_{TDC} P_{TDC} + K_{TT} P_{TT} + K_{H_2} P_{H_2} + K_{NP} P_{NP}. \quad (8)$$

Because the numbers of active sites involved in the RDSs of the dehydrogenations of TDC, CDC, and TT are 2, 2 and 2, the exponents appearing in the denominator of rate equations  $r_1$ ,  $r_2$ , and  $r_3$  should all be 2 for the reverse reactions  $r'_1$ ,  $r'_2$ , and  $r'_4$  as well.

Assuming dissociative desorption of hydrogen in the RDS on Pt active sites, as in case I, the hydrogen term in the denominator becomes  $(K_{H_2} P_{H_2})^{1/2}$ . Moreover, the exponents appearing in the denominators of the foregoing rate equations should all be 3, corresponding to three active sites involved in the RDS.

The acid sites of  $\gamma$ -alumina catalyze the isomerization of *cis*- and *trans*-decalin isomers. The rate of the formation of *trans*-isomer from *cis*-decalin is

$$r_4 = k_{sr4} K'_{CDC} P_{CDC} / \Omega. \quad (9)$$

The rate of the reverse reaction is

$$r'_4 = k'_{sr4} K'_{TDC} P_{TDC} / \Omega. \quad (10)$$

The denominator  $\Omega$  in the foregoing rate equations is

$$1 + K'_{\text{TDC}} P_{\text{TDC}} + K_{\text{CDC}} P_{\text{CDC}}. \quad (11)$$

In Scheme 1, the equations defining the net rate of formation for the various components are

$$\begin{aligned} R_{\text{TDC}} &= r_1 - r'_1 - r_4 + r'_4, \\ R_{\text{CDC}} &= r_2 - r'_2 + r_4 - r'_4, \\ R_{\text{TT}} &= r_1 - r'_1 + r_2 - r'_2 + r'_3 - r_3, \\ R_{\text{NP}} &= r_3 - r'_3. \end{aligned} \quad (12)$$

The set of steady-state continuity equations for the reacting components in a plug-flow reactor can be written as

$$\frac{dX_i}{dW/F_i^0} = R_i, \quad i = 1, \dots, 4, \quad (13)$$

where  $X_1$  and  $X_2$  represent the conversions of TDC and CDC, and  $X_3$  and  $X_4$  their conversion into TT and NP.  $F_i^0$  represents the feed rate of TDC when  $i = 1$ , of CDC when  $i = 2$ , and the total feed rate of TDC + CDC when  $i = 3$  and 4.

#### 4.4. Parameter estimation

The integral method was used for the kinetic analysis [15]. The foregoing set of differential equations was numerically integrated by a fourth-order Runge–Kutta method to yield the reactor effluent composition. Values for the model parameters were estimated by means of regression methods. When the experimental errors were normally distributed with mean 0, the parameters were estimated by minimization of the following multiresponse objective function:

$$S = \sum_{j=1}^m \sum_{l=1}^m W_{jl} \sum_{i=1}^n (y_{ij} - \hat{y}_{ij})(y_{il} - \hat{y}_{il}), \quad (14)$$

where  $m$  is the number of responses,  $n$  is the number of experiments, and the  $w_{jl}$ 's are elements of the inverse of the covariance matrix of the experimental errors on response  $y$ . These can be estimated from replicated experiments. Because the equations are nonlinear in the parameters, the parameter estimates were obtained by minimizing the objective function by Marquardt's algorithm for multiple responses. The foregoing model has 22 parameters. The parameter estimation was performed simultaneously on all of the data obtained at all temperatures by directly substituting the temperature dependence of the parameters into the corresponding rate equations:

for the rate coefficient,

$$k_i = A_i \exp(-E_i/RT); \quad (15)$$

for the adsorption constant,

$$K_i = A_i \exp(\Delta H_i/RT). \quad (16)$$

Models based on adsorption or desorption as RDSs were easily discarded for apparent lack of fit. The discrimination among rival models with surface reactions as RDSs was based on the

Table 1  
Residual sum of squares (RRS) along with the calculated  $F$  values for different models

Model	Residual sum of squares	$F$ values
Case 1-1	0.095	2312
Case 1-2	0.085	2570
Case II-1	0.46	444
Case II-2	0.16	1394

requirement for all the parameters to be positive and statistically significant, and on the residual sum of squares (RRS) as a test for the fit of the data.

The RRS along with the calculated  $F$  values (the ratio of the regression sum of squares to the residue sum of squares) for the rival models are listed in Table 1. Apparently, the two models of case I based on simultaneous removal of three hydrogens fit the experimental data better than those of case II. In case I, there is a slight improvement in the fit of the data for the model with dissociative desorption of hydrogen in the RDS with respect to that with molecular desorption in the RDS. Student's  $t$ -test shows that all of the parameters in both models of case I are statistically significant. The discrimination between the two models of case I also is based on studies showing convincingly that chemisorption of hydrogen is more likely to be a dissociative process [16–18]. Finally, the model of case I-2, based on dissociative desorption of hydrogen in the RDS on Pt sites and on surface reaction as the RDS with the simultaneous removal of three hydrogen molecules, was retained. The excellent fit is also illustrated by the parity plots of Fig. 7, including all of the experiments performed over the entire temperature range.

Table 2 lists the 22 parameter estimates generated by the Fortran program using the Levenberg–Marquardt algorithm for this retained model.

According to Everett [19], the standard entropy change for Langmuir adsorption is given by

$$\Delta S_a^0 = S_a^0 - S_g^0, \quad (17)$$

where  $S_g^0$  is the entropy in the gas phase, taken at unit pressure, and  $S_a^0$  is the entropy in the adsorbed state on the catalyst surface. Mears and Boudart [20] and Trimpont et al. [21] formulated two strict rules for Langmuir adsorption that must be satisfied by  $\Delta S_a^0$ ,

$$-\Delta S_a^0 > 0 \quad (18)$$

and

$$-\Delta S_a^0 < S_g^0, \quad (19)$$

as well as two relations that can be used as guidelines to assess the meaningfulness of the values obtained for  $\Delta S_a^0$  and  $\Delta H_a^0$ ,

$$-\Delta S_a^0 > 42 \quad (20)$$

and

$$-\Delta S_a^0 \leq 51 - 1.4\Delta H_a^0. \quad (21)$$

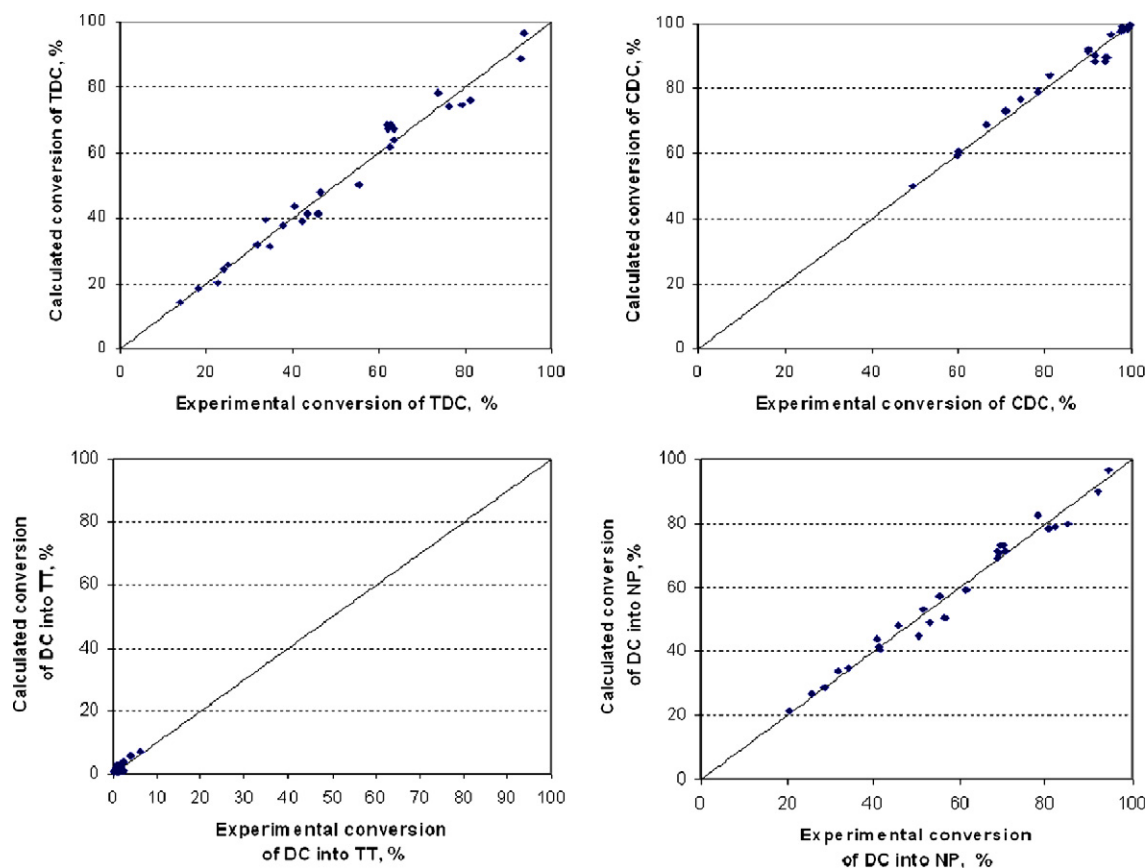


Fig. 7. Parity plots for the various conversions of decalin.

Table 2  
Estimates of frequency factors  $A$ , activation energies  $E$  and enthalpies of adsorption  $\Delta H$  for the model of case I-2 using the Levenberg–Marquardt algorithm

Name of parameter	95%-confidence limits			$t$ -value
	Estimate	Lower	Upper	
$A_{TDC}$	1.54906D+00	1.36662D+00	1.73150D+00	1.69813D+01
$A_{CDC}$	7.89457D+00	6.72133D+00	9.06782D+00	1.34577D+01
$A_{TT}$	9.33959D+01	8.33666D+01	1.03425D+02	1.86246D+01
$A_{MP}$	2.26323D+00	2.07828D+00	2.44819D+00	2.44732D+01
$A_H$	3.31108D+00	3.03161D+00	3.59054D+00	2.36957D+01
$A_{TDC}'$	2.21726D+02	1.96869D+02	2.46582D+02	1.78404D+01
$A_{CDC}'$	4.08540D+01	3.43210D+01	4.73870D+01	1.25070D+01
$A_{TDC\_TT}$	3.63431D+05	3.30382D+05	3.96480D+05	2.19936D+01
$A_{CDC\_TT}$	8.27101D+04	7.43813D+04	9.10389D+04	1.98612D+01
$A_{TT\_HP}$	3.35724D+03	2.85790D+03	3.85659D+03	1.34466D+01
$A_{CDC\_TDC}$	1.24695D+01	1.04767D+01	1.44624D+01	1.25141D+01
$-\Delta H_{TDC}$	1.28343D+04	1.22783D+04	1.33903D+04	4.61677D+01
$-\Delta H_{CDC}$	4.41280D+03	4.04248D+03	4.78313D+03	2.38323D+01
$-\Delta H_{TT}$	3.88825D+03	3.54760D+03	4.22890D+03	2.28285D+01
$-\Delta H_{HP}$	1.07247D+04	1.01217D+04	1.13277D+04	3.55708D+01
$-\Delta H_H$	6.54869D+03	6.02799D+03	7.06938D+03	2.51536D+01
$-\Delta H_{TDC}'$	1.42062D+04	1.27176D+04	1.56947D+04	1.90872D+01
$-\Delta H_{CDC}'$	6.89845D+03	6.17407D+03	7.62283D+03	1.90466D+01
$E_{TDC\_TT}$	2.34547D+04	2.27024D+04	2.42070D+04	6.23572D+01
$E_{CDC\_TT}$	9.05243D+03	8.17648D+03	9.92838D+03	2.06689D+01
$E_{TT\_HP}$	7.06251D+03	6.00993D+03	8.11509D+03	1.34194D+01
$E_{CDC\_TDC}$	2.84393D+04	2.28637D+04	3.40148D+04	1.02014D+01

Note.

$$F = \frac{\text{Regression sum of squares}}{\text{Residual sum of squares}} = \frac{\sum_{j=1}^m \sum_{l=1}^m W_{jl} \sum_{i=1}^n \hat{y}_{ij} \hat{y}_{il} / p}{\sum_{j=1}^m \sum_{l=1}^m W_{jl} \sum_{i=1}^n (y_{ij} - \hat{y}_{ij})(y_{il} - \hat{y}_{il}) / (mn - p)} = 2570.$$

Table 3  
Standard adsorption entropies for the model of case I-2

	$-\Delta S_a^0$ (J/(mol K))
$-\Delta S_{aTDC}^0$	548
$-\Delta S_{aCDC}^0$	539
$-\Delta S_{aTT}^0$	482
$-\Delta S_{aNP}^0$	460
$-\Delta S_{aH}^0$	121
$-\Delta S_{aTDC'}^0$	422
$-\Delta S_{aCDC'}^0$	437

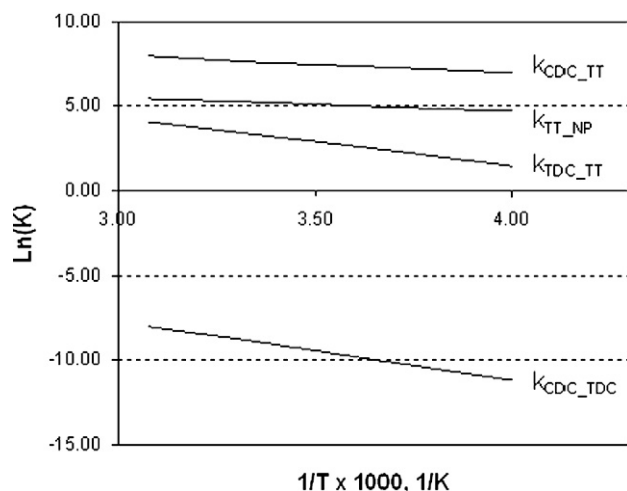


Fig. 8. Arrhenius plot of rate coefficients for the model of case I-2.

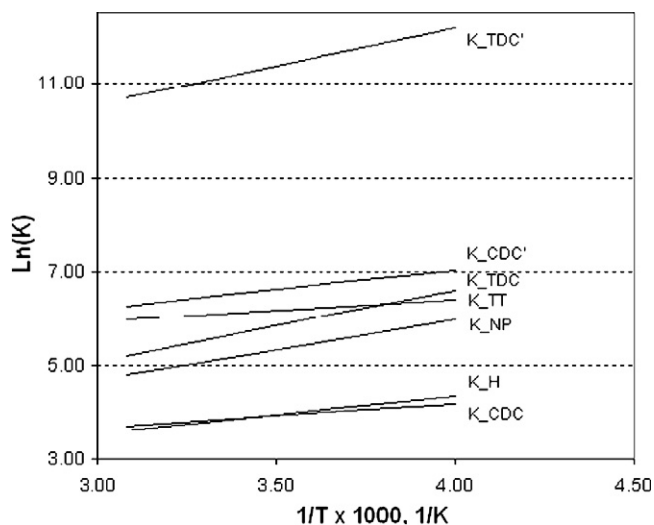


Fig. 9. Van't Hoff plot of adsorption coefficients for the model of case I-2.

All of the adsorption enthalpies reported in Table 2 are negative, as expected. The standard entropies for the model of case I-2, calculated based on (17), are listed in Table 3. These meet all four requirements (18)–(21).

Figs. 8 and 9 show Arrhenius and van't Hoff plots of the rate and adsorption coefficients in the retained model. The rate coefficients increased, but the adsorption coefficients decreased, with increasing temperature. As an example, Figs. 4 and 5 com-

pare the experimental conversions versus space-time and experimental conversions versus the  $H_2$ /decalin molar ratio at 325 °C with the values calculated using the retained model.

## 5. Conclusion

The work reported here illustrates that decalin can be a serious candidate for use as hydrogen carrier. Its dehydrogenation into naphthalene selectively yields pure hydrogen, and the catalyst deactivation is slow. A rigorous kinetic model was derived with the purpose of providing a tool for the design and optimization of the dehydrogenation/hydrogenation process. It accounted for a relatively complex reaction network involving isomerization of the decalin isomers on acid sites, followed by dehydrogenation into naphthalene on Pt active sites and proceeding over tetralin. All of the reactions were shown to be reversible. The rate equations were written in terms of the Hougen-Watson approach, explicitly accounting for the adsorption of the various components of the reaction mixture. The model led to a good fit of the experimental data, with all of the parameters being statistically significant and satisfying the physicochemical constraints.

## Acknowledgments

Financial support was provided by the Department of Energy, Office of Basic Energy Sciences, Division of Chemical Sciences/Geosciences/Biosciences, Catalysis and Chemical Transformations Program, and the Robert A. Welch Foundation.

## Appendix A. List of symbols

Primes on the rates refer to reverse reactions

TDC	<i>trans</i> -decalin
CDC	<i>cis</i> -decalin
TT	tetralin
NP	naphthalene
$D_e$	diffusivity, $cm^2/s$
$A_i$	frequency factor for elementary reaction step $i$ , $kmol/(kg_{cat} h)$
$A_C$	frequency factor for formation of the deactivating agent, $kmol/(kg_{cat} bar^4 h)$
$C_i$	molar concentration of component $i$ , $kmol/m^3$
$C_C$	deactivating agent content of the catalyst, $kg_{CC}/kg_{cat}$
$d_t$	internal tube diameter, $m_r$
$d_p$	particle diameter, $m_p$
$W/F_{0DC}$	space time in terms of decalin feed, $kg_{cat} h/kmol$
$E_i$	activation energy for elementary reaction step $i$ , $kJ/kmol$
$F_{DC}^0$	molar feed rate of reactants decalin, $kmol/h$
$F_i$	molar feed rate of reactant $i$ , $kmol/h$
$F_t$	total molar feed rate, $kmol/h$
$-\Delta H$	heat of reaction, $J/mol$
$-\Delta S_a^0$	standard adsorption entropy, $J/(mol K)$
$S_a^0$	entropy in the gas phase, $J/(mol K)$

$S_g^0$	entropy in the adsorbed state, J/(mol K)
$k_i$	reaction rate coefficient, kmol/(kg <sub>cat</sub> h)
$K_i$	adsorption equilibrium constant, bar <sup>-1</sup>
$L$	volume to surface area of the pellet, m <sub>p</sub>
$r_i$	rate of elementary reaction step $i$ , kmol/(kg <sub>cat</sub> h)
$R_i$	net rate of formation for the component $i$ , kmol/(kg <sub>cat</sub> h)
$T$	temperature, K or °C
$T_m$	mean temperature, K
$R$	gas constant, kJ/(kmol K)
$X_{TDC}$ , $X_{CDC}$	conversion of TDC and CDC, respectively
$X_{TT}$ , $X_{NP}$	conversion of DC into TT and NP, respectively
$Z$	axial reactor coordinate, m <sub>r</sub>

## References

- [1] P. Zegers, J. Power Sources 154 (2006) 497.
- [2] H.L. Hellman, R.V.D. Hoed, Int. J. Hydrogen Energy 32 (2007) 305.
- [3] J.H. Wee, K.Y. Lee, J. Power Sources 157 (2006) 128.
- [4] U.B. Demirci, J. Power Sources 169 (2007) 239.
- [5] M. Farooque, H.C. Maru, J. Power Sources 160 (2006) 827.
- [6] J.R. Ross, Catal. Today 100 (2005) 151.
- [7] Q. Ming, T. Healey, L. Allen, P. Irving, Catal. Today 77 (2002) 51.
- [8] R.B. Biniwale, N. Kariya, M. Ichikawa, Catal. Lett. 105 (2005) 83.
- [9] N. Kariya, A. Fukuoka, T. Utagawa, M. Ichikawa, Appl. Catal. A 247 (2003) 247.
- [10] S. Hodoshima, H. Arai, Y. Saito, Int. J. Hydrogen Energy 28 (2003) 197.
- [11] Y. Okada, E. Sasaki, E. Watanabe, S. Hyodo, H. Nishijima, Int. J. Hydrogen Energy 31 (2006) 1348.
- [12] Y.G. Wang, N. Shah, G.P. Huffman, Energy Fuels 18 (2004) 1429.
- [13] Y.G. Wang, N. Shah, F.E. Huggins, G.P. Huffman, Energy Fuels 20 (2006) 2612.
- [14] Y.K. Park, F.H. Ribeiro, G.A. Somorjai, J. Catal. 178 (1998) 66.
- [15] G.F. Froment, K.B. Bischoff, Chemical Reactor Analysis and Design, second ed., Wiley, New York, 1992.
- [16] S. Wilke, M. Scheffler, Phys. Rev. B 53 (1996) 4926.
- [17] A.T. Gee, B.E. Hayden, C. Mormiche, T.S. Nunney, J. Chem. Phys. 112 (2000) 7660.
- [18] J.R. Kitchin, J.K. Norskov, M.A. Barteau, J.G. Chen, J. Chem. Phys. 120 (2004) 10240.
- [19] D.H. Everett, Trans. Faraday Soc. 46 (1950) 942.
- [20] D.E. Mears, M. Boudart, AIChE J. 12 (1966) 313.
- [21] P.A. Trimpont, G.B. Marin, G.F. Froment, Appl. Catal. 24 (1986) 53.